Proceedings of the DIS'2004, Štrbské Pleso, Slovakia

RESULTS FROM PHENIX ON DEUTERON AND ANTI-DEUTERON PRODUCTION IN AU+AU COLLISIONS AT RHIC

JOAKIM NYSTRAND
FOR THE PHENIX COLLABORATION
Department of Physics and Technology
University of Bergen, Allégaten 55, 5007 Bergen, Norway
E-mail: Joakim.Nystrand@ift.uib.no

Results from the PHENIX Collaboration on the production of deuterons and anti-deuterons in collisions between gold nuclei at a nucleon-nucleon center-of-mass energy of $\sqrt{s_{NN}} = 200$ GeV are presented.

At the Relativistic Heavy Ion Collider (RHIC) at Brookhaven National Laboratory, protons and gold nuclei have been brought to collide at nucleon-nucleon center-of-mass energies up to $\sqrt{s_{NN}} = 200$ GeV. The data this presentation is based on are from Au+Au interactions at the maximum RHIC energy and were accumulated during the second run at RHIC in the year 2001. The results on deuteron and anti-deuteron production from this run have already been submitted for publication[1]. In this talk, these results will be summarized and some of the experimental details not covered in the submitted publication will be discussed.

The PHENIX experiment is a versatile system of detectors aimed at studying a variety of observables in heavy ion interactions. The main parts are two central tracking arms, centered around mid-rapidity, and two muon arms at forward/backward rapidities. Each central tracking arm covers $\Delta\phi = 90^o$ in azimuth and $|\eta| \leq 0.35$ in pseudorapidity ($\eta = \ln(\tan(\Theta/2))$, where Θ is the emission angle). Zero-degree calorimeters (ZDC) and Beam-beam Cherenkov counters (BBC) are used for triggering and event selection. Further details about PHENIX can be found in [2].

The detectors used for this analysis are, in addition to the BBCs and ZDCs, the drift- and pad-chambers (DC and PC) and the Time-of-Flight detector (ToF) from one of the central arms. Tracking and momentum reconstruction of charged particles is provided by the information from the DC and PC. The flight-time measurement from the ToF is combined with the starting time (t0) from the BBC to determine the particle velocity. Figure 1 (left) shows a scatter plot of $q \cdot (1-\beta)$ vs. $1/p$ for reconstructed tracks. Here, q is the electric charge of the reconstructed particle in units of e, β the velocity in units of c, and p the reconstructed momentum. In addition to pion, kaons and protons, bands corresponding to deuterons and anti-deuterons can easily be identified. From β and p, the particle mass, m, can be calculated; Figure 1 (right) shows the distribution for positive and negative particles.

The yields of deuterons and anti-deuterons are obtained by fitting the m^2 distri-

 © Institute of Experimental Physics SAS, Košice, Slovakia

bution to the sum of a gaussian (representing the signal) and an exponential (representing the background) function, as described in [1]. The fits were performed in 7 bins in p_T in the range $1.1 \leq p_T \leq 4.3$. The total number of reconstructed deuterons and anti-deuterons for three centrality selections is listed in Table 1.

Centrality	Number of Events	$< N_{part} >$	Reconstructed deuterons	Reconstructed anti-deuterons
Min. Bias	$21.6 \cdot 10^6$	109.1±4.1	3140	1510
0-20 %	$4.7 \cdot 10^6$	279.9±4.0	1850	870
20-92 %	$16.9 \cdot 10^6$	61.9±3.2	1330	650

Table 1. The number of events, the mean number of participants, and the number of reconstructed deuterons and anti-deuterons for three centrality selections. The number of reconstructed (anti-)deuterons was obtained from separate fits for each centrality selection and p_T bin. This is the reason why the numbers for the subsamples do not add up exactly to the numbers for the min. bias sample. The yields are consistent if the errors from the fits are taken into account.

The corrections needed to convert the raw yields to normalized deuteron/anti-deuteron spectra are obtained by running simulated tracks through a GEANT 3.21 based Monte Carlo simulation program of the detector[3]. For hadrons, this simulation includes particle decay (if applicable), multiple Coulomb scattering, hadronic interactions, and the acceptance, efficiency and resolution of the detector.

The hadronic interactions in Geant 3.21 are handled by FLUKA[4]. Although the implementation of nucleus-nucleus interactions in FLUKA is in progress[5], the version used by Geant 3.21 does not include such processes. The correction for hadronic interactions of (anti-)deuterons thus has to be implemented separately.

The information on what tracking media and corresponding materials lie between the primary vertex and the ToF was extracted from the PHENIX simulation program using 'geantinos', a virtual, non-interacting particle defined in GEANT. A total of 1000 geantinos were generated, originating from the primary vertex and hitting the ToF uniformly distributed over the surface.

From the path lengths, l_i, and densities, n_i, of the different materials, and the corresponding cross sections σ_i, the probability that a particle should survive

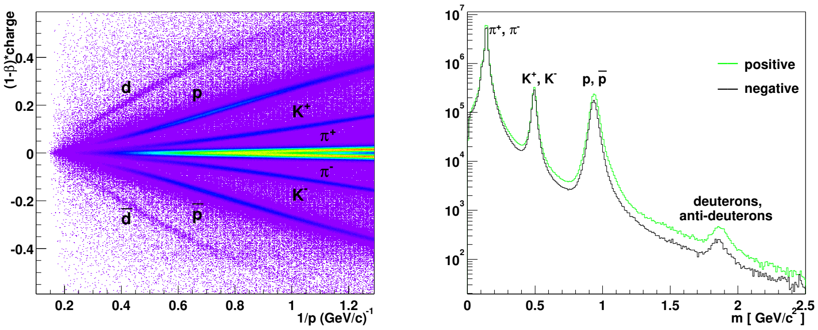

Figure 1. Left: Scatter plot of $q \cdot (1-\beta)$ vs. $1/p$ for tracks in the central tracking arm. Right: Yield as a function of mass for positive and negative particles.

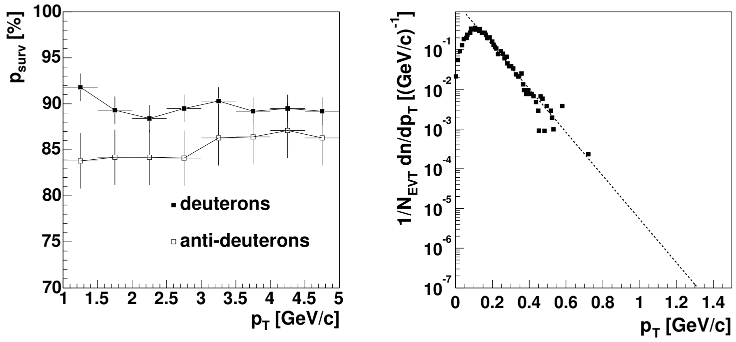

Figure 2. Left: The probability as a function of transverse momentum that an (anti-)deuteron will reach the ToF without undergoing any inelastic hadronic interaction. The limited statistics in the GEANT simulation is partly responsible for the scattering of the points. Right: Transverse momentum distribution of knock-out deuterons from the detector material. The dotted line is an exponential fit[8].

without suffering any hadronic interaction is given by

$$\exp(-\sum_i \sigma_i n_i l_i) \ . \tag{1}$$

The experimental data on total cross sections for deuteron induced interactions are limited, and there are of course no data on anti-deuteron induced interactions. A direct parameterization of $\sigma(d+A)$ or $\sigma(\overline{d}+A)$ is therefore not possible. Instead, a method has been developed which calculates the (anti-)deuteron inelastic cross sections from the (anti-)proton and (anti-)neutron cross sections. For σ_{pA}, $\sigma_{\overline{p}A}$, σ_{nA}, and $\sigma_{\overline{n}A}$, the parameterizations in [6] are used.

The effective nucleon-nucleus cross section is calculated as the average of the neutron- and proton-nucleus cross sections, $\sigma_{NA} = (\sigma_{pA} + \sigma_{nA})/2$, and similarly for anti-nucleons. Based on the geometry of a nuclear collision, the deuteron cross section is then written

$$\sigma_{dA} = [\sqrt{\sigma_{NA}} + \Delta_d(A)]^2 \ . \tag{2}$$

$\Delta_d(A)$ corresponds to the average difference in radius between a nucleon and a deuteron and can thus be expected to be largely independent of nuclear mass number and collision energy. Comparisons with deuteron data[7] shows that a constant $\Delta_d(A) = 3.51 \pm 0.25$ mb$^{1/2}$ can be used.

Using the parameterizations of σ_{pA} and $\sigma_{\overline{p}A}$, the hadronic interaction probabilities of (anti-)protons were first calculated from Eq. 1. This calculation was then compared with the interaction probabilities calculated from GEANT/FLUKA. The difference between the two methods was small. The final nucleon interaction probabilities were calculated as the mean of the two methods, and the difference was used as an estimate of the systematic error. The ratio of the hadronic interaction probabilities of (anti-)deuterons to those of (anti-)protons were then calculated using the cross sections from Eq. 2 in Eq. 1. These ratios depend on the size of the target; for (anti-)protons with momenta of 0.75 GeV/c they are $d/p = 1.79$,

$\overline{d}/\overline{p} = 1.34$ for hydrogen targets and $d/p = 1.43$, $\overline{d}/\overline{p} = 1.16$ for copper targets, for example. The resulting ratios (d/p, $\overline{d}/\overline{p}$) were applied to the nucleon interaction probabilities. The final hadronic survivabilities for deuterons and anti-deuterons are plotted in Figure 2 (left).

The simulation of the experimental acceptance is done for single particles in the detector. The effect of high occupancy has been investigated by embedding simulated particles in real events. The result is corrections of 6.9±2.7%, 19.8±7.1%, and 2.2±3.1% for min. bias (0-92%), central (0-20%), and non-central (20-92%) collisions, respectively. The embedding corrections are largely independent of p_T.

Finally, possible background sources must be investigated. For anti-deuterons, this is not a problem; any anti-deuterons seen in the detector must have been produced in the primary collision between the two gold nuclei. Deuterons, however, can be produced in secondary (knock-out) reactions between the produced particles and the detector material. This has been investigated by running simulated Au+Au events from Hijing through the GEANT simulation program. The rate of production of secondary deuterons, primarily from interactions in the beam-pipe and the PHENIX Multiplicity Vertex Detector, is indeed quite high, but, as can be seen in Figure 2 (right), the yield is concentrated at very low transverse momenta. It is estimated that the contribution from knock-out deuterons in the lowest p_T-bin ($1.1 \leq p_T \leq 1.5$ GeV/c) is less than 0.1%. No corrections for background deuterons have therefore been applied.

The results after corrections are shown as normalized invariant yields in Figure 3. The spectra from the central and non-central samples have been fit to a Boltzmann distribution for a narrow interval in rapidity,

$$\frac{d^2n}{p_T dp_T dy} = C \cdot m_T \cdot e^{-m_T/T} \ , \tag{3}$$

over the range $1.1 \leq p_T \leq 3.5$ GeV/c. These fits give temperatures of 452 ± 23 MeV

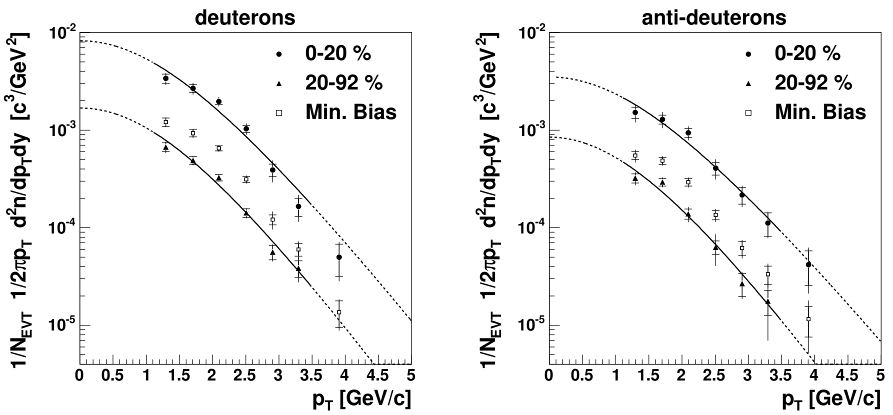

Figure 3. Invariant yield of deuterons and anti-deuterons as a function of transverse momentum for three centrality selections. The error bars show the total error (quadratic sum of stat. and syst.) The horizontal bars show the statistical errors.

(0-20%) and 421 ± 21 MeV (20-92%) for deuterons and 475 ± 37 MeV (0-20%) and 412 ± 31 MeV (20-92%) for anti-deuterons.

These temperatures are considerably higher than what has been observed for anti-deuterons produced in pp collisions at $\sqrt{s} = 53$ GeV. A fit to the combined data of [9] in the range $0.15 \leq p_T \leq 1.0$ GeV/c gives $T = 110 \pm 26$ MeV.

By extrapolating the Boltzmann fits (dashed curves in Fig. 3) the mean transverse momentum at mid-rapidity can be calculated. The $< p_T >$ of pions, kaons, and protons[3] are compared with that of (anti-)deuterons in Figure 4 (left). As can be seen, the $< p_T >$ of (anti-)deuterons is much higher than for the lighter particles. The results are well described by a linear function in the particle mass:

$$< p_T > = < p_T >_0 + \beta \cdot mc \; . \tag{4}$$

A fit gives $< p_T >_0 = 358$ MeV/c and $\beta = 0.65$. The large values of $< p_T >$ for (anti-)deuterons clearly indicate that they get a large fraction of their energy from the collective radial flow produced in central nucleus-nucleus collisions. This is what one would naïvely expect from the trend seen for the lighter particles in Fig. 4. It is, however, difficult to see how the (anti-)deuterons with a binding energy of only 2.2 MeV can survive the intense hadronic rescattering normally assumed to produce the strong radial flow.

The (anti-)deuterons produced at mid-rapidity in nuclear collisions at the current energy may be formed through neutron-proton coalescence at the late stages of the collisions. If one assumes that neutrons and protons (anti-neutrons and anti-protons) have the same phase space distribution, the invariant yield of deuterons

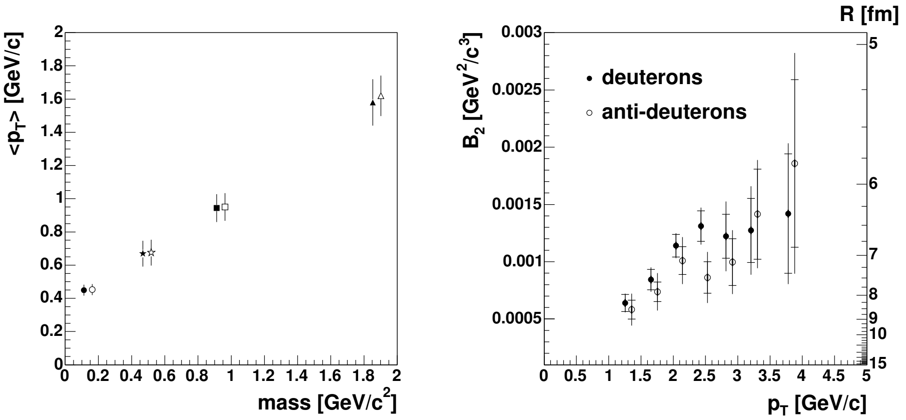

Figure 4. Left: Mean transverse momentum vs. particle mass for pions, kaons, protons, and deuterons in central collisions. Solid and open symbols correspond to positively and negatively charged particles, respectively. To separate the two, the particle masses have been slightly shifted. The errors are in all cases dominated by the systematic errors. Right: The coalescence parameter B_2 as a function of p_T for central collisions. The R values on the right-hand y-axis are from Eq. 6. The error bars are defined as in Fig. 3.

(anti-deuterons) is given by

$$E_d \frac{d^3n}{dp_d^3} = B_2 \left(E_p \frac{d^3n}{dp_p^3} \right)^2 \tag{5}$$

where B_2 is the coalescence parameter for mass number A=2 and $p_p = p_d/2$. It should be noted that for B_2 = constant, the coalescence model leads to approximately the same mean p_T for protons and deuterons, $< p_T >_d \approx < p_T >_p$ (this relation is strictly true if the protons have an exponential distribution in p_T, $dn/p_T dp_T \propto \exp(-p_T/T)$). If one assumes that the nucleons before freeze-out are uniformly distributed within a (static) sphere with radius R, B_2 can be related to R through (assuming $m_T \approx 2m$)

$$R = \left(\frac{9\pi^2}{2} \frac{(\hbar c)^3}{m_p \cdot B_2 \cdot c^5} \right)^{1/3} . \tag{6}$$

B_2 for central collisions is plotted in Figure 4 (right) as a function of transverse momentum; the corresponding values of R are plotted on the right-hand y-axis. The (anti-)proton spectra from[3] are corrected for the contribution from weak decays before B_2 is calculated[1]. Eq. 6 gives a source radius near that of a gold nucleus. The increase of B_2 with p_T and the observed large $< p_T >$ of (anti-)deuterons are, however, not consistent with a static source, and clearly point to the importance of collective flow. This estimate of R can therefore only provide the correct order of magnitude.

To summarize, PHENIX has measured the production of deuterons and anti-deuterons at mid-rapidity in gold-gold collisions at RHIC. The results show that the transverse momentum of the (anti-)deuterons primarily originates in the strong radial flow, despite the small deuteron binding energy. The invariant yields of (anti-)deuterons are not consistent with emission from a static source.

References

1. S. S. Adler *et al.* [PHENIX Collaboration], arXiv:nucl-ex/0406004, submitted to Phys. Rev. Lett.
2. K. Adcox *et al.* [PHENIX Collaboration], Nucl. Instrum. Meth. A **499** (2003) 469 and references therein.
3. S. S. Adler *et al.* [PHENIX Collaboration], Phys. Rev. C **69** (2004) 034909 [arXiv:nucl-ex/0307022].
4. A. Fasso, A. Ferrari, P. R. Sala and J. Ranft, SLAC-REPRINT-2000-117 *Prepared for Int. Conf. on Advanced Monte Carlo for Radiation Physics, Particle Transport Simulation and Applications (MC 2000), Lisbon, Portugal, 2000.*
5. A. Fasso *et al.*, eConf **C0303241** (2003) MOMT005 [arXiv:hep-ph/0306267].
6. A.A. Moiseev, J.F. Ormes Astroparticle Physics **6** (1997) 379.
7. J. Jaros *et al.*, Phys. Rev. C **18** (1978) 2273; E.O. Abdurakhmanov *et al.*, Z. Phys. C **5** (1980) 1.
8. R. du Rietz, Lic. Thesis, Lund University (2003).
9. B. Alper *et al.*, Phys. Lett. B **46** (1973) 265; S. Henning *et al.* [British-Scandinavian-MIT Collaboration], Lett. Nuovo Cim. **21** (1978) 189.